# H3K27me3 regulates BMP activity in developing spinal cord

**Naiara Akizu[1], Conchi Estarás[1], Laura Guerrero[1], Elisa Martí[2] and Marian A. Martínez-Balbás[1]#**

[1] Department of Genomic Regulation. [2] Department of Developmental Biology. Instituto de Biología Molecular de Barcelona (IBMB), Consejo Superior de Investigaciones Científicas (CSIC), Baldiri i Reixac 15-21, Parc Científic de Barcelona, E-08028 Barcelona, Spain

**#Corresponding author:**

E-mail: mmbbmc@ibmb.csic.es

Tel.: +34 93 4034961

Fax: +34 93 4034979

**Running title**: Autoregulation of BMP pathway by H3K27me3

**Keywords:** Neural development/BMP pathway/Epigenetic regulation/Histone methylation/ EZH2/JMJD3

**SUMMARY**

**During spinal cord development the combination of secreted signaling proteins and transcription factors provide information for each neural type differentiation. Studies using embryonic stem cells show that trimethylation of lysine 27 of histone H3 (H3K27me3) contributes to repression of many genes key for neural development. However, it remains unclear how H3K27me3-mediated mechanisms control neurogenesis in developing spinal cord. Here we demonstrate that H3K27me3 controls dorsal interneuron generation by regulation of BMP activity. Our study indicates that Noggin expression, a BMP extracellular inhibitor, is repressed by H3K27me3. Moreover, we show that Noggin expression is induced by BMP pathway signaling, generating a negative feedback regulatory loop. In response to BMP pathway activation, JMJD3 histone demethylase interacts with Smad1/Smad4 complex to demethylate and activate Noggin promoter. Together our data reveal how BMP signaling pathway restricts its own activity in developing spinal cord by modulating H3K27me3 levels at Noggin promoter.**

## INTRODUCTION

During embryogenesis, multipotent neuroepithelial precursor cells originate specialized neurons and different glial cell types (Gage, 2000; Roegiers and Jan, 2004; Temple, 2001). Whether a precursor cell either self-renews or differentiates is regulated by interactions between transcription factors and secreted signaling proteins that provide positional information (Jessell, 2000; Zhu and Scott, 2004). Bone Morphogenetic Proteins (BMP) are some of these extracellular proteins. In developing spinal cord, BMPs regulate several processes such as differentiation to dorsal interneurons (Liu and Niswander, 2005; Timmer et al., 2002). These differentiation processes require nuclear reorganization and general changes in gene expression, indicating that epigenetic changes may be involved (Buszczak and Spradling, 2006; Hsieh and Gage, 2005; Kondo, 2006). One of the best-illustrated epigenetic effects on regulation of pluripotency and differentiation induction is the effect mediated by Polycomb repressive complexes (PRC) (Ringrose and Paro, 2007). The hallmark for Polycomb-mediated repression is the methylation of lysine 27 of histone H3 (H3K27me3) (Czermin et al., 2002; Muller et al., 2002). Enhancer of Zeste Homolog 2 (EZH2), a subunit of the PRC2 complex, is responsible for histone methyltransferase activity (Cao et al., 2002; Czermin et al., 2002; Kuzmichev et al., 2002). This mark is recognized by the chromodomain of Polycomb protein that forms part of the PRC1 (Cao et al., 2002). The recruitment of PRC1 leads to final transcriptional repression that is reversible by JMJD3 and UTX demethylase activity (Agger et al., 2007; De Santa et al., 2007; Lan et al., 2007; Lee et al., 2007). The balance between methyltransferase and demethylase activity gives a dynamic character which is reflected by the fact that many key developmental promoters are often marked by H3K27me3 (Boyer et al., 2006;

Bracken et al., 2006; Lee et al., 2006; Pan et al., 2007). In addition to H3K27me3, an active modification, H3K4me, is often found at these promoters (Bernstein et al., 2006; Mikkelsen et al., 2007; Pan et al., 2007; Zhao et al., 2007). It is believed that the presence of both activating and repressive chromatin marks keeps these developmental regulators poised for rapid resolution after the appropriate stimulus is received (Bernstein et al., 2006).

Many models have been used to examine epigenetic changes that take place during cell differentiation and, in particular, to analyze the role of Polycomb complexes using embryonic stem cells (ESC) (Boyer et al., 2006; Bracken et al., 2006; Lee et al., 2006; Pietersen and van Lohuizen, 2008). However, these systems generally do not progress toward a specific terminal cell type as it occurs in vivo. In this paper we take advantage of an in vivo model for neurogenesis, the chick embryo neural tube, to analyze the role of H3K27me3 during nervous system development.

Here we report an H3K27me3-mediated mechanism to edge the boundaries of BMP activity during spinal cord development. We show that expression of Noggin, an extracellular inhibitor of BMPs, is regulated by H3K27me3. As a consequence, a reduction of H3K27me3 disturbs BMP-regulated dorsal spinal cord development. Moreover, we show that H3K27me3-mediated Noggin repression is sensitive to changes in BMP activity. Hyperactivation of BMP signaling pathway induces JMJD3 interaction with Smad1/Smad4 and their recruitment to Noggin promoter for H3K27me3 demethylation that triggers Noggin expression. Our results reveal an essential role of H3K27me3 in the negative feedback regulation of BMP signaling that guarantees proper neurogenesis in developing chick neural tube.

## MATERIALS AND METHODS

**Plasmids and recombinant proteins**

Human EZH2 and its deleted form lacking SET domain (aminoacid 622-707) were cloned from pCDNA3 (Caretti et al., 2004) into pCIG vector (Megason and McMahon, 2002), upstream of an internal ribosomal entry site (IRES) and three nuclear localization sequences-tagged EGFP. Human Myc-JMJD3 and Myc-JMJD3DN (H1390A truncated JMJD3) (Xiang et al., 2007) were cloned into pCIG. Mouse BMP4/7, chick Shh (Roberts et al., 1998) and human FlagSmad1 (Liu et al., 1996) were also cloned into pCIG. Mouse Wnt1, chick Noggin and human HaSmad4 are described elsewhere (Alvarez-Medina et al., 2008; Garcia-Campmany and Marti, 2007). DNA sequences for chick Noggin shRNA and a random shRNA (shRNA C-) were cloned into pSHIN vector (Kojima et al., 2004). Noggin shRNA target sequence: 5'gtggctctggtcccagacc3'. Random sequence: 5'gctccacatcagtccttcc3'

**Chick in ovo electroporation**

Eggs from White-Leghorn chickens were incubated at 38.5ºC and 70% humidity. Embryos were staged following Hamburger and Hamilton (HH) (Hamburger and Hamilton, 1992). Chick embryos were electroporated with purified plasmid DNA at 0.25-3 µg/µl in $H_2O$ with 50 ng/ml of Fast Green. Plasmid DNA was injected into the lumen of HH10 or HH16 neural tubes, electrodes were placed at both sides of the neural tube and embryos were electroporated by an IntracelDual Pulse (TSS-100) electroporator delivering five 50 ms square pulses of 20-25 V.

**Antibodies**

Antibodies used were: anti-BrdU, anti-Pax7, anti-ISL1/2 (DSHB), anti-neural b-Tubulin III (Tuj1), anti-Pax6 (Covance), anti-LHX2/9 (from TM Jessell), anti-trimethylH3K27, anti-acetylH3 (K9 and K14), anti-acetylH4 (K12), anti-di/trimethylH3K4, anti-trimethylH4K20, anti-phosphoH3S10 (Upstate Biotechnology), anti-EZH1 (kindly

provided by Dr. Reinberg), anti-trimethylH3K9 (Abcam, UK), anti-HA (Sigma H6908), anti-Flag (Sigma M2), anti-phosphoSmad1/5/8 (Cell signaling), anti-myc ChIP Grade (Abcam) and anti-myc (from Dr. S. Pons).

**Indirect immunofluorescence**

The collected embryos' brachial regions were fixed for 2h at 4ºC in 4% paraformaldehyde, rinsed, sunk in PBS 30% sucrose solution and embedded in OCT for sectioning in LEICA cryostat (CM 1900). Sections were blocked at room temperature for 1h in 1% bovine serum albumin (in PBS with 0.1% TritonX) before overnight (O/N) incubation at 4ºC with primary antibodies. Finally, sections were incubated for 2h at room temperature with Alexa-conjugated goat secondary IgG antibodies (Jackson Immuno Research Inc.) and 0.1 ng/µl DAPI (Sigma). Images were captured by Leica SP5 confocal microscope using LAS-AF software. Fluorescence intensity was quantified using Leica LAS-AF software.

**Histone extraction and Immunoblotting**

HH14 and HH25 wild-type (WT) embryos were collected and neural tubes were dissected out. For histone acid extraction, neural tubes were incubated for 30 min at 4ºC in lysis buffer (Hepes/kOH 10 nM, $MgCl_2$ 1.5 mM, KCl 10 mM, DTT 0.5 mM, PMSF 1.5 mM, TSA 0.33 µM, HCl 0.2 N). After centrifugation for 10 min at 13,400 rpm, supernatant was collected and dialysis was done, with acetic acid 0.1 M and miliQ $H_20$, using slide-A-lyzer mini dialysis units (Pierce). Histone concentration was measured with Bradford protein assay reagent and 10 µg of proteins were separated in SDS-PAGE gel. Immunoblotting was performed with standard procedures and visualized by ECL kit (Amersham).

**BrdU incorporation**

0.5 µg/ml bromodeoxyuridine (BrdU) was injected into the chick embryo neural tube lumen 30 min before fixation. BrdU was detected on sections by treatment with HCl2 N for 30 min, NaBorate 0.1 M (pH 8.5) and incubation with anti-BrdU antibody.

**In situ hybridization (ISH)**

Embryos were fixed overnight at 4ºC in 4% paraformaldehyde, rinsed and processed for whole-mount RNA ISH , following standard procedures using ESTbank probes for chick EZH2, JMJD3, Hes5, NeuroD, NeuroM, Noggin, ID1 and ID3. After hybridization, embryos were post-fixed in paraformaldehyde 4% for 2h, embedded in sucrose 10%, agarose 5% solution and sectioned in a Leica vibratome (VT 1000S).

**Fluorescent associated cell sorting (FACS)**

Electroporated embryos were dissected out and trypsinized for 5-10 min in Trypsin-EDTA 0.5% (Sigma). Trypsinization was stopped with 20% horse serum in PBS-0.1% glucose solution. GFP+ cells from cell suspension were sorted by flow cytometry using a MoFlo flow cytometer (DakoCytomation, Fort Collins, CO).

**Cell cycle analysis**

Trypsinized cell suspension from electroporated neural tubes was treated 2h at room temperature with 10 µg/ml Hoescht33342. Hoescht and GFP fluorescence were determined by flow cytometry using a MoFlo flow cytometer (DakoCytomation, Fort Collins, CO). DNA content analysis (Ploidy analysis) was done using Multicycle software (Phoenix Flow Systems, San Diego, CA).

**Microarrays analysis**

Fifteen chick embryo neural tubes were electroporated with empty vector or EZH2DSET for each replicates. RNA-s from 100,000 FACS-purified GFP+ cells of each replicate were supplied to IRB's Affymetrix Facility for quality control, quantification, reverse transcription, labeling and hybridization onto Affymetrix

Chicken GeneChip. Results in CEL files were provided to the Bioinformatics and Data Analysis service of UB-SCT, for analysis of data quality, normalization with the RMA algorithm and selection of differentially expressed genes (absolute fold change >1.5 in both replicates).

**mRNA extraction and quantitative PCR (qPCR)**

mRNA from FACS-separated cells or from dissected neural tubes was extracted by TRIZOL (Invitrogen) protocol with 2 µl of pellet paint co-precipitant (Novagene). Reverse transcription was performed with Transcriptor kit (Roche), following the manufacturer's procedure. qPCR was performed with Sybergreen (Roche) in LC480 Lightcycler (Roche). GapdH was used for normalization. Primer sequences: Noggin FW5'gctacagtaaaaggtcttgctc3'; RW5'cctcaggatcgttaaatgcac3'; Hes5 FW5'taaaccataactcaagctgtgtag3'; RW5'gcatacatatcctgaacctcac3'; NeuD FW5'actacttgttacctttcccg3'; RW5'atggtttaaaataggaaatccacg3'; Id1 FW5'tgaagggctgctactcg3'; RW5'aggtcccagatgtagtcg3'; Id3 FW5'cgactgctactccaaattgc3'; RW5'gaagatataatcgatgacgtgctg3'.

**Chromatin immunoprecipitation (ChIP)**

For histone ChIPs 300,000-400,000 cells separated by FACS or 2-3 dissected neural tubes, were used. ChIPs were performed essentially as described elsewhere (Attema et al., 2007). Cells were treated with formaldehyde 1% at room temperature for 10 min. The reaction was stopped with 125 mM glycine. Cells were washed once in ice-cold PBS with protease inhibitors and lysed with 50 µl lysis buffer [SDS 1%, EDTA 10 mM, Tris 50 mM (pH 8), protease inhibitors 1 µg/ml, PMSF 1 mM], incubated 5 min on ice and diluted with 150 µl PBS before 10 min sonication in biorruptor (Novagene) (High power, 30 sec ON, 1 min OFF). 200-500bp chromatin fragments containing supernatant was precleared with 8 µl of proteinA agarose/ssDNA beads (Upstate 16-157) for 30 min

at 4ºC under rotation. Supernatant was recovered by centrifugation and input was separated. The rest of the chromatin was diluted with IP buffer [Triton X-100 1%, EDTA 2 mM, NaCl 150 mM, Tris 20 mM (pH 8) and protease inhibitors] and divided into three eppendorfs. 2 µg of antibodies or IgG were added O/N incubation at 4ºC under rotation. Antibody:protein:DNA complexes were then collected with 10 µl of proteinA agarose/ssDNA beads for 1h. The beads were washed with buffers I [SDS 0.1%, Triton X-100 1%, EDTA 2 mM, Tris-HCl 20 mM (pH 8), NaCl 150 mM], II [SDS 0.1%, Triton X-100 1%, EDTA 2mM, Tris-HCl 20 mM (pH 8), NaCl 500 mM], III [LiCl 0.25 M, NP40 1%, NaDOC 1%, EDTA 1mM, Tris-HCl 10 mM (pH 8)], and three times with Tris-EDTA. Washed pellets were eluted with 400 µl of SDS 1%, NaHCO3 0.1 M solution and de-crosslinked O/N at 65ºC. DNA was recovered by using phenol chloroform extraction and ethanol precipitation.

For non histone proteins ChIPs were performed as described above with some modifications: 400,000-500,000 cells separated by FACS or 20-25 dissected electroporated side of neural tubes, were fixed at room temperature 45 min with DSG 2 mM (Sigma) and 20 min with formaldehyde 1%. Cells were lysed with 1.1 ml lysis buffer [SDS 0.1%, EDTA 1 mM, Tris 20 mM (pH 8), Triton X-100 1%, NaCl 150 mM, protease inhibitors 1 µg/ml, PMSF 1 mM]. After immunoprecipitation beads were washed with buffers I (SDS 0.1%, NaDOC 0.1%, Triton X-100 1%, EDTA 1 mM, HEPES 20 mM, NaCl 150 mM), II (SDS 0.1%, NaDOC 0.1%, Triton X-100 1%, EDTA 1 mM, HEPES 20 mM, NaCl 500 mM), III (LiCl 250 mM, NP40 0.5%, NaDOC 0.5%, EDTA 1mM, HEPES 20 mM), and IV (EDTA 10 mM, HEPES 200 mM).

DNA was analyzed by qPCR with Sybergreen (Roche) in LC480 (Roche). Primer sequences are: Noggin(-2000) FW5’cttgcgatgctttttgtgac3’, RW5’cgtggagcagttttacagac3’; Noggin(-1000) FW5’gggtagggtgggttagaaga3’,

RW5'ccaaagcctttaaatttcctgc3'; Noggin(+300) FW5'gctacagtaaaaggtcttgctc3', RW5'cctcaggatcgttaaatgcac3'; Hes5(-2000) FW5'tgaaagattggcagaggaaac3', RW5'gtacccatttctcactacagc3'; NeuD(-2000) FW5'ttccgtaatcgtgtgtactcg3', RW5'atttagttaatggaaaagacatcgc3'.

**Cell culture, transfection and Coimmunoprecipitation (CoIP) assay**

Hek293T cells were grown in DMEM with 10% fetal calf serum and 1% Penicillin/Streptomycin at 37°C, 5% CO2. Cells were transfected by a standard calcium phosphate co-precipitation protocol and harvested 48h after transfection. Immunoprecipitations and immunoblot analysis were performed essentially as described elsewhere (Valls et al., 2003).. Immunoblotting was performed using standard procedures and visualized using ECL kit (Amersham).

**Identification of Smad binding sequences in the Noggin promoter region**

Sequence comparison of the Noggin locus between Human and Chicken was performed using the global alignment programme Shuffle-LAGAN (Brudno et al., 2003) and visualized with VISTA visualization tool (Mayor et al., 2000). Smad conserved binding sites were found using rVISTA 2.0 searches for Smad matrix from the TRANSFAC library.

**Statistical analysis**

Quantitative data were expressed as mean and standard deviation (s.d.). Significant differences between groups were tested by Student's *t*-test.

## RESULTS

### H3K27me3 global levels increase during neural differentiation

To understand the contribution of histone marks in neural development, we examined their distribution throughout early development. We studied the pattern of

histone acetylation and methylation in HH14 and HH25 chick embryo neural tubes. While in HH14 embryos the neural tube is mainly formed by proliferating neuroblasts in HH25 embryos two zones are distinguished: the ventricular zone (VZ) formed by proliferating neuroblasts and the mantle zone (MZ) where differentiated neurons reside (Fig. 1A). First, we analyzed histone marks along neurogenesis by immunoblotting of histones purified from neural tubes. While global histone acetylation and H3K4me2/3 levels were similar in HH14 and HH25 embryo neural tubes (Supplementary Fig. 1A), clear increase in global H3K27me3 was detected from stage HH14 to stage HH25 (Fig. 1B). This correlates not only with neurogenesis progression but also with enrichment in differentiated neurons. Then, we tested whether H3K27me3 levels were higher in differentiated neurons than in proliferating neuroblasts. By HH25 embryo neural tubes immunostaining we observed that global H3K27me3 levels were 3 times higher in differentiated neurons (MZ) than in neuroblasts (VZ) (Fig. 1C). These data indicate that global H3K27me3 levels increase along neurogenesis, while differentiated neurons accumulate in the neural tube. Similar results were observed for H3K9me3 and for H4K20me3 (Supplementary Fig. 1B).

The observed global H3K27me3 level increase led us to analyze the expression of the two mayor enzymes responsible for H3K27me3, EZH2 and JMJD3. Transversal sections of HH10 and HH14 embryo ISH show that EZH2 and JMJD3 are ubiquitously expressed in the neural tube, although their expression level is higher in the dorsal region (Fig. 1D,E). At HH25 neural tubes, EZH2 and JMJD3 are highly expressed in VZ while the mRNA levels of both enzymes in MZ are lower. Moreover the VZ expression of EZH2 and JMJD3 is higher at dorsal neuroblasts, resulting in a well defined dorsal JMJD3 domain and a dorsoventral EZH2 gradient (Fig. 1D,E). The EZH2 and JMJD3 expression pattern suggests that H3K27me3 could be more

dynamically controlled in VZ neuroblasts, especially at dorsal region. However, it doesn't completely correlate with global H3K27me3 increase during neural differentiation. Thus, we analyzed the expression of EZH1, whose histone methyltransferase (HMT) activity has been recently described (Margueron et al., 2008; Shen et al., 2008). Supplementary Fig. 1C shows that EZH1 expression is higher in differentiated neurons than in proliferating neuroblasts at HH30 embryo neural tubes. This result suggests that in addition to EZH2 and JMJD3, EZH1 contributes to the H3K27me3 levels maintaining at differentiated neurons.

**Maintenance of global H3K27me3 is not required for neural differentiation or for progenitor proliferation**

Consistent with the observed global H3K27me3 levels increase during neural differentiation (Fig. 1B,C) recent evidences demonstrates that PcG proteins and H3K27me3 are present at promoters of many genes specific for neurogenesis (Boyer et al., 2006; Lee et al., 2006; Pietersen and van Lohuizen, 2008). Therefore, we investigated whether a global H3K27me3 increase is required for neurogenesis (although this does not necessarily reflect a requirement of H3K27me3 at a particular chromatin locus). To address this possibility we reduced global H3K27me3 levels in the chick neural tube to next analyze the effects on neural differentiation. In order to reduce H3K27me3 levels, chick embryo neural tubes were in ovo electroporated with a dominant negative form of EZH2 (EZH2DSET), which lacks the SET domain responsible for HMT activity. First, we tested the ability of EZH2DSET to block endogenous EZH activity. Fig. 2A shows that EZH2DSET over-expression (GFP+ cells) reduces by 70% endogenous H3K27me3 levels 24h post-electroporation (PE). H3K27me3 is maintained at low levels for 48h, but it starts to recover 72h-PE

(Supplementary Fig. 2A). EZH2 over-expression caused no change in global H3K27me3 levels (Fig. 2A). Similarly, no changes in global H3K9me3 or H3K4me3 levels were detected after EZH2DSET over-expression (Supplementary Fig. 2B,C). Once global H3K27me3 levels were reduced in chick neural tube, we examined its role in neural differentiation by analyzing the expression of NeuroD and NeuroM, proneural genes expressed in differentiating neurons and previously identified as H3K27me3 targets in ESC (Boyer et al., 2006; Lee et al., 2006). To this end, EZH2DSET, EZH2 or the empty vector were electroporated in HH10 embryo neural tubes, when the neural tube is mainly formed by proliferating neuroblasts. No changes in the expression levels of NeuroD and NeuroM differentiation markers were detected after H3K27me3 reduction (Supplementary Fig. 3A). To confirm these results, we checked the pan-neural differentiation marker Tuj. Embryos transfected with EZH2DSET and stained for Tuj does not show changes in the number of differentiated cells neither at 48h nor at 72h-PE (Fig. 2B and Supplementary Fig. 4A). These results indicate that global H3K27me3 maintenance is not essential to neural differentiation; the observed global H3K27me3 increase during neurogenesis might be a consequence of the differentiation process itself, in which extensive structural changes in chromatin are known to take place over all the genome (Keenen and de la Serna, 2009). In line with this hypothesis, other heterochromatin marks, such as H3K9me3 and H4K20me3, also increase during neurogenesis (Supplementary Fig. 1B).

The high EZH2 and JMJD3 expression at the VZ suggests that a dynamic control of H3K27me3 might be important in neuroblast proliferation. Moreover, EZH2 and H3K27me3 regulate several proliferating processes (Agger et al., 2009; Bracken et al., 2003; Ezhkova et al., 2009; Varambally et al., 2002). Then, we analyzed the function of H3K27me3 in the maintenance of the proliferating neuroblast population.

To this end, EZH2DSET, EZH2 or the empty vector were electroporated in HH10 embryo neural tubes and the effect on neuroblast proliferation and cell cycle progression was analyzed. Immunostaining using H3S10p antibody shows that electroporated and control sides of the neural tubes have the same number of mitotic cells (Supplementary Fig. 3B). We also evaluated neural tube cells entry into S-phase of the cell cycle: when electroporated embryos were pulse-labeled with BrdU, no differences were observed between EZH2DSET, EZH2 or empty vector electroporations neither at 24h nor at 72h-PE (Fig. 2C and Supplementary Fig. 4B). Finally, by GFP+ DNA content analysis, no changes on cell cycle phase distribution were observed after global H3K27me3 decrease (Supplementary Fig. 3C and Supplementary Fig. 4C). Taken together, these findings suggest that global H3K27me3 levelmaintenance is not essential to neuroblast proliferation.

**H3K27me3 regulates BMP activity**

Next, we examined whether the observed dorsoventral expression gradient of EZH2 and JMJD3 (Fig. 1D,E) has any physiological significance in the neural tube dorsoventral pattern formation. We analyzed the development of dorsal neural populations by immunostaining of Lhx2/9 and Isl1/2 dorsal interneuron markers, after H3K27me3 reduction (by EZH2DSET over-expression). Lhx2/9 and Isl1/2 positive dorsal interneuron populations decrease in EZH2DSET electroporated side of the neural tubes (Fig. 3A). It is well established that BMP pathway is the main factor responsible for dorsal patterning of the neural tube (Liu and Niswander, 2005; Timmer et al., 2002). Then, we examined whether low levels of H3K27me3 affect BMP activity. To this end, we activated the BMP pathway by in ovo electroporation of BMP expression vector in the presence or absence of EZH2DSET. The expression pattern of Pax6/7 genes, known

to be regulated by BMP activity (Liu and Niswander, 2005), was analyzed by immunostaining. Fig. 3B shows that BMP activity leads to a ventral expansion of Pax6/7 domains that is counteracted by H3K27me3 reduction after EZH2DSET over-expression. This result indicates that H3K27me3 is required to maintain proper BMP activity in the developing spinal cord.

**BMP activity is regulated by Noggin induction via H3K27 demethylation**

To understand how H3K27me3 regulates BMP activity, we performed a micro-array analysis comparing GFP+ cells purified by FACS from EZH2DSET or empty vector electroporated neural tubes (Fig. 4A left panel). Differentially upregulated genes after H3K27me3 removal (by EZH2DSET electroporation) were analyzed by Gene Ontology (GO). 22 upregulated genes were associated with seven GO biological process terms related to nervous system development (Fig. 4A right panel). Interestingly, we found among them Noggin, a known BMP inhibitor (Zimmerman et al., 1996). As confirmed by qPCR, Noggin is upregulated (1.9±0.6-fold) in EZH2DSET-transfected neural tube cells (Fig. 4B), suggesting that Noggin upregulation could be responsible for the phenotype described above.

In order to examine whether changes in Noggin expression are directly associated with H3K27me3 levels, HH16-18 embryo neural tubes were dissected out and H3K27me3 ChIP analysis were performed. In addition to Noggin, NeuroD and Hes5 promoters, which are not transcriptionally affected by H3K27me3 reduction (Fig. 4B), were also analyzed. Hes5 was used as a negative control of ChIP analysis, as it is highly expressed in neural tubes (ISH in Fig. 4C) and, thus, it is expected not to be enriched in H3K27me3. NeuroD, a known H3K27me3 target in ESC (Boyer et al., 2006; Lee et al., 2006) and repressed in analyzed neural tubes (ISH in Fig. 4C) was used

as positive control of H3K27me3 ChIP. Fig. 4C shows that Noggin promoter, which is transcriptionally inactive in most of the neural tube cells, is enriched in H3K27me3 nucleosomes (7.2±2.5 % of input), although this enrichment is smaller than in the NeuroD promoter (22.1±7.5 % of input). As expected, Hes5 promoter H3K27me3 levels are in the same range of mock ChIP (Fig. 4C).

Next, GFP+ cells from neural tubes electroporated in ovo with empty vector or with EZH2DSET were sorted by FACS and H3K27me3 levels at Noggin, NeuroD and Hes5 promoters were analyzed by ChIP assays. Results in Fig. 4D show that, after EZH2DSET expression, H3K27me3 levels decrease at both, Noggin promoter (2.8±1.2 fold) and NeuroD promoter (2.1±0.01 fold), though only Noggin is activated (Fig. 4B). Many promoters of key development regulators bear, in addition to H3K27me3, the active H3K4me mark (Bernstein et al., 2006; Mikkelsen et al., 2007; Pan et al., 2007; Zhao et al., 2007). It has been hypothesized that these marks' combination creates a poised state suitable for rapid induction (Bernstein et al., 2006). To find whether the presence of H3K4me together with H3K27me3 contributes to gene expression regulation, we tested the presence of this histone modification at the three gene promoters analyzed previously. Fig. 4C shows that in HH16-18 embryo neural tube cells, Hes5, Noggin and NeuroD promoters are enriched in H3K4me2 (Fig. 4C; 14.8±1.3, 6.±2.7, 3.1±1.5 % of input respectively). H3K4me2 levels at Noggin promoter are similar to H3K27me3 ones, while at NeuroD promoter H3K4me2 levels are clearly lower than H3K27me3 levels (Fig. 4C right diagram). ChIP assays analyzed by qPCR show that H3K4me2 is not affected by EZH2DSET over-expression (Fig. 4D). However, loss of H3K27me3 levels at Noggin promoter, leads to a predominance of H3K4me2 over H3K27me3. The contrary happens at NeuroD promoter where H3K27me3 is maintained above H3K4me2 levels even after the H3K27me3 reduction

by EZH2DSET over-expression. These ratios correlate well with Noggin and NeuroD expression levels observed after H3K27me3 reduction (Fig. 4D right diagram).

**Noggin transcription is regulated by BMP pathway**

Then, we asked whether Noggin upregulation upon a signal induction requires H3K27me3 removal. To establish the activity responsible for Noggin regulation, BMP, Wnt and Shh signaling pathways were activated and Noggin mRNA levels were determined by qPCR and ISH. Results in Fig. 5A show a clear Noggin induction 24h after BMP electroporation (20.19±7.6-fold BMP7; 44.0±7.6-fold BMP4). A 7.1±1.2 fold increase of Noggin expression is already observed 6h after BMP electroporation (Supplementary Fig. 5A). In addition, electroporation of constitutively active Smad1 (one of the BMP pathway effectors) also induces Noggin expression (Supplementary Fig. 5B). Next, we analyzed whether this activation is associated with changes in H3K27me3 at Noggin promoter. To do this, HH10 neural tubes electroporated in ovo with BMP were dissected out 24h-PE and analyzed by ChIP assays. Fig. 5B shows that BMP induced Noggin activation correlates with 3.3±2 fold decrease of H3K27me3 and a 1.6±0.003 fold increase of H3K4me2. Consequently, the resulting H3K4me2/H3K27me3 relative levels at Noggin promoter reach those observed at transcriptionally active Hes5 promoter (Fig. 5B right panel). Furthermore, H3K4me3, a histone modification associated to transcriptionally activated genes (Barski et al., 2007), increases 2.11±0.33 fold close to transcriptional start site of Noggin after BMP induction (Supplementary Fig. 6). Together, these data suggest that active H3K27me3 demethylation of Noggin promoter takes place upon BMP signaling activation. JMJD3 has been described as an H3K27me3 specific demethylase. Moreover, it has been suggested that JMJD3 activity could be associated to an H3K4 methyltransferase

activity (Lim et al., 2009). Therefore, we wondered whether JMJD3 histone demethylase (HDM) activity is involved in BMP-dependent Noggin induction. To answer this question, neural tubes were electroporated with BMP together with an empty vector or a dominant negative form of JMJD3 (JMJD3DN) that lacks HDM activity. Electroporated neural tube cells were separated by FACS to next analyze Noggin mRNA and promoter H3K27me3 levels. Fig. 5C shows that Noggin mRNA level is 1.7±0.2 fold lower when JMJD3DN is overexpressed correlating with 1.8±0.2 higher H3K27me3 level at Noggin promoter. These results suggest that JMJD3 contributes to BMP-induced Noggin expression. Then, we tested if JMJD3 interacts to Noggin promoter upon BMP pathway activation. To that end, neural tubes were electroporated with an empty vector, myc-JMJD3 or myc-JMJD3 with BMP. Electroporated neural tube cells were separated by FACS and the presence of JMJD3 at Noggin promoter was analyzed by ChIP assays, using myc antibody. Results show 1.7±0.035 fold higher JMJD3 recruitment to Noggin promoter upon BMP signaling activation (Fig. 5C). On the other hand, immunoprecipitated chromatin levels are similar for myc-JMJD3 alone and for the empty vector electroporated neural tube cells. This indicates that in the absence of BMP hyperactivation (when Noggin is repressed in most of the neural tube cells) JMJD3 is not recruited to Noggin promoter. In agreement with this result, JMJD3 over-expression, which effectively reduces global H3K27me3 levels (Supplementary Fig. 7A), has no significant effect on Noggin expression (Supplementary Fig. 7B), nor on H3K27me3 levels at the Noggin promoter (Supplementary Fig. 7C). All together, these data suggest that BMP pathway activates Noggin promoter through JMJD3-mediated H3K27 demethylation.

Then, we sought to determine whether a direct link exists between BMP signaling pathway effectors and JMJD3. Smad1 is a BMP pathway effector (Liu and

Niswander, 2005). Upon BMP signaling activation Smad1 is phosphorylated and interacts with Smad4 to enter into the nucleus. Once in the nucleus, Smad1/Smad4 heterodimer regulates its target genes interacting with co-activator or co-repressor proteins (Liu and Niswander, 2005). Fast BMP-induced Noggin expression (Supplementary Fig. 5A) and evidences of conserved Smad response-element presence at Noggin promoter (Supplementary Fig. 5C) suggest that Noggin could be a direct target of Smad1/Smad4. To test this hypothesis, HH10 neural tubes electroporated with BMP were dissected out 24h-PE and analyzed by ChIP using pSmad1/5/8 antibody. Fig. 6A shows that BMP-induced Noggin activation correlates with endogenous phospho-Smad1 recruitment (2.3±0.3 fold increase) to Noggin promoter. The observed effects of JMJD3 on BMP-induced Noggin expression (Fig. 5C) as well as the association of active Smad1 (Fig. 6A) and JMJD3 (Fig. 5C) at Noggin promoter upon BMP pathway activation led us to test whether Smad1/Smad4 interacts with JMJD3. CoIP experiments indicate that JMJD3 interacts with Smad1/Smad4 complex (Fig. 6B,C,D). Fig. 6B shows that Smad1 interacts with JMJD3 only in the presence of Smad4. Smad4 binding to JMJD3 also requires the presence of Smad1 (Fig. 6C). Moreover, Smad1/Smad4-JMJD3 interaction increases after BMP pathway activation (Fig. 6D). All these data suggest that upon BMP pathway activation, Smad1/Smad4 heterodimer recruits JMJD3 histone demethylase to Noggin promoter. This targeting results in a decrease of H3K27me3 levels that correlates with gene transcription activation.

Finally, we sought to analyze whether BMP-dependent upregulation of Noggin plays any role controlling BMP activity. To do that, HH10 neural tubes were electroporated with BMP and shRNA for Noggin (that partially reduces BMP-induced Noggin expression, Supplementary Fig. 8A) or BMP and shRNA control. They were dissected out 24h-PE and electroporated cells (GFP+) were separated by FACS for

mRNA extraction. Then we tested whether the reduction of Noggin levels affect BMP activity by analyzing mRNA levels of Id3 [a well known BMP transcriptional target (Hollnagel et al., 1999)] by qPCR and ISH. Fig. 7A shows that coelectroporation of BMP and Noggin shRNA leads to a 2.2±1.1 fold higher Id3 mRNA levels compared to BMP and shRNA control electroporation. Similar results were observed for Id1 (Supplementary Fig. 8B). Moreover, Noggin over-expression leads to a reduction of Lhx2/9 and Isl1 dorsal interneurons, regulated by endogenous BMP pathway activity (Supplementary Fig. 8C). All together, these data strongly suggest that BMP-induced Noggin activation modulates BMP activity in the neural tube.

**DISCUSSION**

Our studies have uncovered new insights into the in vivo role of H3K27me3 mark in the context of lineage establishment within a tissue. We have shown that this epigenetic mark regulates dorsal patterning in developing neural tube by repressing Noggin promoter. BMPs are needed for the formation of dorsal neural cell types (Liu and Niswander, 2005). Thus, regulation of BMP activity by expression of BMP inhibitors plays an important role in this process. Our studies suggest a model in which Noggin, a known BMP antagonist, is regulated by an H3K27me3-dependent mechanism in the developing spinal cord (Fig. 7B). Noggin, is repressed in most of the developing neural tube cells. This repression requires H3K27me3 at Noggin promoter (1). In response to high BMP activity, Smad1/Smad4 and JMJD3 are recruited to Noggin promoter that in turn demethylates this promoter (2). H3K27me3 decrease, together with H3K4me increase, leads to Noggin full induction (3), which in turn rapidly moderates high BMP activity (4). This may occur in the most caudal developing spinal

cord, in which Noggin is expressed at dorsal cells to finally fine-tune levels of BMP activity along the anterior-posterior axis of the neural tube (Fig. 7B).

Interestingly, EZH2 and JMJD3 expression is higher at dorsal cells at the analyzed stages of neural tube development. This coincides with both high BMP (Sela-Donenfeld and Kalcheim, 2002) and dorsal Noggin expression (Fig. 7B) in the developing neural tube. These observations support the role of H3K27me3 in the BMP-dependent generation of dorsal neural subtypes described in our study. On the other hand, both EZH2 and JMJD3 are expressed in the VZ of the neural tube, and their mRNA levels are reduced in the MZ occupied by differentiated neurons. The loss of EZH2 expression during differentiation is a common feature, as it has been described in in vitro neural differentiation models (Sher et al., 2008) or during epidermal development (Ezhkova et al., 2009). Nonetheless it does not explain the observed global H3K27me3 increase during neural differentiation. These data suggest that in addition to EZH2 and JMJD3, other enzymes might be responsible for global H3K27me3 in the developing neural tube. According to this, high global H3K27me3 levels found in differentiated neurons could be maintained by observed high EZH1 expression at differentiated neurons. This correlates with the data supporting that EZH1 is the main responsible for HMT activity in differentiated tissues (Margueron et al., 2009).

In agreement with the proposed role for H3K27me3 in development, our studies have uncovered a distinct promoter behavior in response to H3K27me3 removal that might be critical to determine the promoter activity in response to the developmental decisions. Our data show that some H3K27me3 target genes are not activated after H3K27me3 removal (as Neuro D). This observation suggests a context-dependent H3K27me3 function that might rely on the targeting of sequence-specific transcription factors in response to different pathway activation. H3K27me3 mark might ensure that

further developmental decisions are firmly controlled by robust induction signals. In agreement with this, different Polycomb and H3K27me3 targets have been identified in transformed human cells (Bracken et al., 2006; Squazzo et al., 2006), undifferentiated stem cells (Pasini et al., 2007) and human T cells (Barski et al., 2007; Roh et al., 2006) in which different signaling pathways operate.

Another possibility to explain the lack of transcriptional consequences after EZH2DSET over-expression implies the chromatin context of H3K27me3 target genes. The fact that Noggin, but not NeuroD, is activated after H3K27me3 removal, even in the absence of any induction signal, suggest that the presence of H3K27me3 should be combined with other chromatin features to fine tune the transcriptional regulation. In ESCs H3K4me active and H3K27me3 repressive marks coexist over many of the lineage-regulatory genes that are governed by PRCs (Haudenschild et al., 2004; Liu and Niswander, 2005; Pasini et al., 2007). They are found in transcriptionally silenced genes and they poise them for activation upon a signal induction (Bernstein et al., 2006). Transcriptional activation of these genes requires an increase on H3K4me over H3K27me3 levels. Our results show that both, Noggin and NeuroD promoters contain active and repressive marks. However only Noggin is activated after H3K27me3 reduction. The ratio between H3K4me2 and H3K27me3 at Noggin promoter is higher than at NeuroD promoter, suggesting this ratio (and not only the presence of both marks) might be determinant in the genes becoming active or repressed at some particular development stage. Therefore our data suggest that H3K27me3/H3K4me2 relative levels might regulate the promoter sensitivity to respond to developmental decisions.

We have shown that small changes in Noggin expression, mediated by discreet changes in H3K27me3 levels of its promoter, lead to altered BMP-regulated dorsal

patterning in the neural tube. Many processes of neural development, like neural induction and axon guidance, are also regulated by BMP signaling (Liu and Niswander, 2005). These processes are temporally and spatially separated along the nervous system development. Thus, the duration and strength of BMP signaling are essential to correct neural development. One way to modulate BMP activity is by the transcriptional activation of its own extracellular antagonists (Haudenschild et al., 2004; Liu and Niswander, 2005). Here we also show that Noggin expression is upregulated fast after BMP over-expression. This upregulation is essential to moderate BMP activity, since the partial blocking of BMP-mediated Noggin induction, increases transcriptional activity of Id1 and Id3 BMP target genes (Hollnagel et al., 1999). Moreover, we demonstrated that Noggin expression is directly regulated by BMP responding Smad proteins (Smad1/5/8). BMP-induced Noggin expression is accompanied by a JMJD3-dependent removal of H3K27me3 from Noggin promoter. The identified JMJD3 interaction with Smad1/Smad4 heterodimer, suggests that they could form a complex responsible for JMJD3 recruitment to Noggin promoter. One question that remains to be answered is whether this mechanism is also working for other BMP target genes.

Our study has uncovered a fine-tuning regulatory mechanism of the BMP pathway where chromatin structure is implicated. We propose that the chromatin structure at Noggin promoter allows a fast response to small BMP activity variations, thus ensuring the proper BMP levels required for nervous system development. A key question is whether this is a developmental-stage specific mechanism that only operates during embryonic development or it can be a more general mechanism. The latter is supported by data showing that both EZH2 and BMPs are implicated in the development of several cancers (Haudenschild et al., 2004; Varambally et al., 2002).

However, further evidence will be required to ascertain the contribution of H3K27me3-mediated BMP regulation in tumorigenesis.

**ACKNOWLEDGEMENTS**

We would like to thank Dr. X. de la Cruz for critically reviewing the paper. We also thank Dr. Pons for reagents, Dr. Sartorelli, Dr. Xiang, Dr Kojima, Dra. Bovolenta and Dr. Briscoe for DNAs and Dr. Reinberg for anti-EZH1 antibody. This study was supported by the grants, SAF2005-01285, BFU2006-01493 and CSD2006-00049 to MAMB and BFU2007 to EM from the Spanish Ministry of Education and Science. NA was recipient of an I3P fellowship (I3P-BPD2005).

**REFERENCES**

**Agger, K., Cloos, P. A., Christensen, J., Pasini, D., Rose, S., Rappsilber, J., Issaeva, I., Canaani, E., Salcini, A. E. and Helin, K.** (2007). UTX and JMJD3 are histone H3K27 demethylases involved in HOX gene regulation and development. *Nature* **449**, 731-734.

**Agger, K., Cloos, P. A., Rudkjaer, L., Williams, K., Andersen, G., Christensen, J. and Helin, K.** (2009). The H3K27me3 demethylase JMJD3 contributes to the activation of the INK4A-ARF locus in response to oncogene- and stress-induced senescence. *Genes Dev* **23**, 1171-1176.

**Alvarez-Medina, R., Cayuso, J., Okubo, T., Takada, S. and Marti, E.** (2008). Wnt canonical pathway restricts graded Shh/Gli patterning activity through the regulation of Gli3 expression. *Development* **135**, 237-247.

**Attema, J. L., Papathanasiou, P., Forsberg, E. C., Xu, J., Smale, S. T. and Weissman, I. L.** (2007). Epigenetic characterization of hematopoietic stem cell differentiation using miniChIP and bisulfite sequencing analysis. *Proc Natl Acad Sci U S A* **104**, 12371-12376.

**Barski, A., Cuddapah, S., Cui, K., Roh, T. Y., Schones, D. E., Wang, Z., Wei, G., Chepelev, I. and Zhao, K.** (2007). High-resolution profiling of histone methylations in the human genome. *Cell* **129**, 823-837.

**Bernstein, B. E., Mikkelsen, T. S., Xie, X., Kamal, M., Huebert, D. J., Cuff, J., Fry, B., Meissner, A., Wernig, M., Plath, K. et al.** (2006). A bivalent chromatin structure marks key developmental genes in embryonic stem cells. *Cell* **125**, 315-326.

**Boyer, L. A., Plath, K., Zeitlinger, J., Brambrink, T., Medeiros, L. A., Lee, T. I., Levine, S. S., Wernig, M., Tajonar, A., Ray, M. K. et al.** (2006). Polycomb complexes repress developmental regulators in murine embryonic stem cells. *Nature* **441**, 349-353.

**Bracken, A. P., Dietrich, N., Pasini, D., Hansen, K. H. and Helin, K.** (2006). Genome-wide mapping of Polycomb target genes unravels their roles in cell fate transitions. *Genes Dev* **20**, 1123-1136.

**Bracken, A. P., Pasini, D., Capra, M., Prosperini, E., Colli, E. and Helin, K.** (2003). EZH2 is downstream of the pRB-E2F pathway, essential for proliferation and amplified in cancer. *EMBO J* **22**, 5323-5335.

**Brudno, M., Malde, S., Poliakov, A., Do, C. B., Couronne, O., Dubchak, I. and Batzoglou, S.** (2003). Glocal alignment: finding rearrangements during alignment. *Bioinformatics* **19 Suppl 1**, i54-62.

**Buszczak, M. and Spradling, A. C.** (2006). Searching chromatin for stem cell identity. *Cell* **125**, 233-236.

**Cao, R., Wang, L., Wang, H., Xia, L., Erdjument-Bromage, H., Tempst, P., Jones, R. S. and Zhang, Y.** (2002). Role of histone H3 lysine 27 methylation in Polycomb-group silencing. *Science* **298**, 1039-1043.

**Caretti, G., Di Padova, M., Micales, B., Lyons, G. E. and Sartorelli, V.** (2004). The Polycomb Ezh2 methyltransferase regulates muscle gene expression and skeletal muscle differentiation. *Genes Dev* **18**, 2627-2638.

**Czermin, B., Melfi, R., McCabe, D., Seitz, V., Imhof, A. and Pirrotta, V.** (2002). Drosophila enhancer of Zeste/ESC complexes have a histone H3 methyltransferase activity that marks chromosomal Polycomb sites. *Cell* **111**, 185-196.

**De Santa, F., Totaro, M. G., Prosperini, E., Notarbartolo, S., Testa, G. and Natoli, G.** (2007). The histone H3 lysine-27 demethylase Jmjd3 links inflammation to inhibition of polycomb-mediated gene silencing. *Cell* **130**, 1083-1094.

**Ezhkova, E., Pasolli, H. A., Parker, J. S., Stokes, N., Su, I. H., Hannon, G., Tarakhovsky, A. and Fuchs, E.** (2009). Ezh2 orchestrates gene expression for the stepwise differentiation of tissue-specific stem cells. *Cell* **136**, 1122-1135.

**Gage, F. H.** (2000). Mammalian neural stem cells. *Science* **287**, 1433-1438.

**Garcia-Campmany, L. and Marti, E.** (2007). The TGFbeta intracellular effector Smad3 regulates neuronal differentiation and cell fate specification in the developing spinal cord. *Development* **134**, 65-75.

**Hamburger, V. and Hamilton, H. L.** (1992). A series of normal stages in the development of the chick embryo. 1951. *Dev Dyn* **195**, 231-272.

**Haudenschild, D. R., Palmer, S. M., Moseley, T. A., You, Z. and Reddi, A. H.** (2004). Bone morphogenetic protein (BMP)-6 signaling and BMP antagonist noggin in prostate cancer. *Cancer Res* **64**, 8276-8284.

**Hollnagel, A., Oehlmann, V., Heymer, J., Ruther, U. and Nordheim, A.** (1999). Id genes are direct targets of bone morphogenetic protein induction in embryonic stem cells. *J Biol Chem* **274**, 19838-19845.

**Hsieh, J. and Gage, F. H.** (2005). Chromatin remodeling in neural development and plasticity. *Curr Opin Cell Biol* **17**, 664-671.

**Jessell, T. M.** (2000). Neuronal specification in the spinal cord: inductive signals and transcriptional codes. *Nat Rev Genet* **1**, 20-29.

**Keenen, B. and de la Serna, I. L.** (2009). Chromatin remodeling in embryonic stem cells: regulating the balance between pluripotency and differentiation. *J Cell Physiol* **219**, 1-7.

**Kojima, S., Vignjevic, D. and Borisy, G. G.** (2004). Improved silencing vector co-expressing GFP and small hairpin RNA. *Biotechniques* **36**, 74-79.

**Kondo, T.** (2006). Epigenetic alchemy for cell fate conversion. *Curr Opin Genet Dev* **16**, 502-507.

**Kuzmichev, A., Nishioka, K., Erdjument-Bromage, H., Tempst, P. and Reinberg, D.** (2002). Histone methyltransferase activity associated with a human multiprotein complex containing the Enhancer of Zeste protein. *Genes Dev* **16**, 2893-2905.

**Lan, F., Bayliss, P. E., Rinn, J. L., Whetstine, J. R., Wang, J. K., Chen, S., Iwase, S., Alpatov, R., Issaeva, I., Canaani, E. et al.** (2007). A histone H3 lysine 27 demethylase regulates animal posterior development. *Nature* **449**, 689-694.

**Lee, M. G., Villa, R., Trojer, P., Norman, J., Yan, K. P., Reinberg, D., Di Croce, L. and Shiekhattar, R.** (2007). Demethylation of H3K27 regulates polycomb recruitment and H2A ubiquitination. *Science* **318**, 447-450.

**Lee, T. I., Jenner, R. G., Boyer, L. A., Guenther, M. G., Levine, S. S., Kumar, R. M., Chevalier, B., Johnstone, S. E., Cole, M. F., Isono, K. et al.** (2006). Control of developmental regulators by Polycomb in human embryonic stem cells. *Cell* **125**, 301-313.

**Lim, D. A., Huang, Y. C., Swigut, T., Mirick, A. L., Garcia-Verdugo, J. M., Wysocka, J., Ernst, P. and Alvarez-Buylla, A.** (2009). Chromatin remodelling factor Mll1 is essential for neurogenesis from postnatal neural stem cells. *Nature* **458**, 529-533.

**Liu, A. and Niswander, L. A.** (2005). Bone morphogenetic protein signalling and vertebrate nervous system development. *Nat Rev Neurosci* **6**, 945-954.

**Liu, F., Hata, A., Baker, J. C., Doody, J., Carcamo, J., Harland, R. M. and Massague, J.** (1996). A human Mad protein acting as a BMP-regulated transcriptional activator. *Nature* **381**, 620-623.

**Margueron, R., Justin, N., Ohno, K., Sharpe, M. L., Son, J., Drury, W. J., 3rd, Voigt, P., Martin, S. R., Taylor, W. R., De Marco, V. et al.** (2009). Role of the polycomb protein EED in the propagation of repressive histone marks. *Nature* **461**, 762-767.

**Margueron, R., Li, G., Sarma, K., Blais, A., Zavadil, J., Woodcock, C. L., Dynlacht, B. D. and Reinberg, D.** (2008). Ezh1 and Ezh2 maintain repressive chromatin through different mechanisms. *Mol Cell* **32**, 503-518.

**Mayor, C., Brudno, M., Schwartz, J. R., Poliakov, A., Rubin, E. M., Frazer, K. A., Pachter, L. S. and Dubchak, I.** (2000). VISTA : visualizing global DNA sequence alignments of arbitrary length. *Bioinformatics* **16**, 1046-1047.

**Megason, S. G. and McMahon, A. P.** (2002). A mitogen gradient of dorsal midline Wnts organizes growth in the CNS. *Development* **129**, 2087-2098.

**Mikkelsen, T. S., Ku, M., Jaffe, D. B., Issac, B., Lieberman, E., Giannoukos, G., Alvarez, P., Brockman, W., Kim, T. K., Koche, R. P. et al.** (2007). Genome-wide maps of chromatin state in pluripotent and lineage-committed cells. *Nature* **448**, 553-560.

**Muller, J., Hart, C. M., Francis, N. J., Vargas, M. L., Sengupta, A., Wild, B., Miller, E. L., O'Connor, M. B., Kingston, R. E. and Simon, J. A.** (2002). Histone methyltransferase activity of a Drosophila Polycomb group repressor complex. *Cell* **111**, 197-208.

**Pan, G., Tian, S., Nie, J., Yang, C., Ruotti, V., Wei, H., Jonsdottir, G. A., Stewart, R. and Thomson, J. A.** (2007). Whole-genome analysis of histone H3 lysine 4 and lysine 27 methylation in human embryonic stem cells. *Cell Stem Cell* **1**, 299-312.

**Pasini, D., Bracken, A. P., Hansen, J. B., Capillo, M. and Helin, K.** (2007). The polycomb group protein Suz12 is required for embryonic stem cell differentiation. *Mol Cell Biol* **27**, 3769-3779.

**Pietersen, A. M. and van Lohuizen, M.** (2008). Stem cell regulation by polycomb repressors: postponing commitment. *Curr Opin Cell Biol* **20**, 201-207.

**Ringrose, L. and Paro, R.** (2007). Polycomb/Trithorax response elements and epigenetic memory of cell identity. *Development* **134**, 223-232.
**Roberts, D. J., Smith, D. M., Goff, D. J. and Tabin, C. J.** (1998). Epithelial-mesenchymal signaling during the regionalization of the chick gut. *Development* **125**, 2791-2801.
**Roegiers, F. and Jan, Y. N.** (2004). Asymmetric cell division. *Curr Opin Cell Biol* **16**, 195-205.
**Roh, T. Y., Cuddapah, S., Cui, K. and Zhao, K.** (2006). The genomic landscape of histone modifications in human T cells. *Proc Natl Acad Sci U S A* **103**, 15782-15787.
**Sela-Donenfeld, D. and Kalcheim, C.** (2002). Localized BMP4-noggin interactions generate the dynamic patterning of noggin expression in somites. *Dev Biol* **246**, 311-328.
**Shen, X., Liu, Y., Hsu, Y. J., Fujiwara, Y., Kim, J., Mao, X., Yuan, G. C. and Orkin, S. H.** (2008). EZH1 mediates methylation on histone H3 lysine 27 and complements EZH2 in maintaining stem cell identity and executing pluripotency. *Mol Cell* **32**, 491-502.
**Sher, F., Rossler, R., Brouwer, N., Balasubramaniyan, V., Boddeke, E. and Copray, S.** (2008). Differentiation of neural stem cells into oligodendrocytes: involvement of the polycomb group protein Ezh2. *Stem Cells* **26**, 2875-2883.
**Squazzo, S. L., O'Geen, H., Komashko, V. M., Krig, S. R., Jin, V. X., Jang, S. W., Margueron, R., Reinberg, D., Green, R. and Farnham, P. J.** (2006). Suz12 binds to silenced regions of the genome in a cell-type-specific manner. *Genome Res* **16**, 890-900.
**Temple, S.** (2001). The development of neural stem cells. *Nature* **414**, 112-117.
**Timmer, J. R., Wang, C. and Niswander, L.** (2002). BMP signaling patterns the dorsal and intermediate neural tube via regulation of homeobox and helix-loop-helix transcription factors. *Development* **129**, 2459-2472.
**Valls, E., de la Cruz, X. and Martinez-Balbas, M. A.** (2003). The SV40 T antigen modulates CBP histone acetyltransferase activity. *Nucleic Acids Res* **31**, 3114-3122.
**Varambally, S., Dhanasekaran, S. M., Zhou, M., Barrette, T. R., Kumar-Sinha, C., Sanda, M. G., Ghosh, D., Pienta, K. J., Sewalt, R. G., Otte, A. P. et al.** (2002). The polycomb group protein EZH2 is involved in progression of prostate cancer. *Nature* **419**, 624-629.
**Xiang, Y., Zhu, Z., Han, G., Lin, H., Xu, L. and Chen, C. D.** (2007). JMJD3 is a histone H3K27 demethylase. *Cell Res* **17**, 850-857.
**Zhao, X. D., Han, X., Chew, J. L., Liu, J., Chiu, K. P., Choo, A., Orlov, Y. L., Sung, W. K., Shahab, A., Kuznetsov, V. A. et al.** (2007). Whole-genome mapping of histone H3 Lys4 and 27 trimethylations reveals distinct genomic compartments in human embryonic stem cells. *Cell Stem Cell* **1**, 286-298.
**Zhu, A. J. and Scott, M. P.** (2004). Incredible journey: how do developmental signals travel through tissue? *Genes Dev* **18**, 2985-2997.
**Zimmerman, L. B., De Jesus-Escobar, J. M. and Harland, R. M.** (1996). The Spemann organizer signal noggin binds and inactivates bone morphogenetic protein 4. *Cell* **86**, 599-606.

## FIGURE LEGENDS

**Figure 1. H3K27me3 global levels increase during neural differentiation**

(A) Diagram showing regions occupied by proliferating progenitors (ventricular zone, VZ) and post-mitotic neurons (mantle zone, MZ) in HH25 and HH14 (only progenitors) chick embryo spinal cord. TZ: transition zone. (B) H3K27me3 levels of HH14 and HH25 embryo spinal cord histone extracts determined by immunoblotting.

(C) Sections from HH25 chick embryos (brachial region) stained with anti-H3K27me3 and DAPI (DNA). The graphic underneath shows mean of H3K27me3/DAPI (DNA) signal intensity in individual cells relative to progenitor mean intensity. Intensities were quantified by Leica LAS-AF software. Data show mean of n=80 cells (from 4 different embryo sections). Error bars indicate s.d. ***$p<0.0001$

(D) EZH2 and (E) JMJD3 mRNA analyzed by HH10, 14 and 25 chick embryos ISH.

**Figure 2. H3K27me3 maintenance is not essential for neural differentiation or for progenitor proliferation**

HH10 embryos were electroporated with EZH2DSET, EZH2 or the empty vector in a bicistronic vector containing GFP.

(A) H3K27me3 immunostaining (grey and red) of 24h post-electroporated (24h-PE) embryos. The graphic shows mean of H3K27me3 signal intensity in EZH2DSET electroporated individual cells (GFP+, green bar), relative to non-electroporated ones (grey bar). Intensities were quantified by Leica LAS-AF software. Data show mean of n=44 cells (from 4 different electroporated embryo sections). Error bars indicate s.d. ***$p<0.0001$.

(B) TUJ immunostaining (grey and red) of 48h-PE embryos.

(C) BrdU immunostaining (grey and red) of 24h-PE embryos. The graphic shows percentage of electroporated cells (GFP+) positive for BrdU. Data show mean of n=30 sections (from 4-6 embryos). Error bars indicate s.d.

**Figure 3. H3K27me3 regulates BMP activity**

(A) LHX2/9 (upper panel) or ISL1/2 (lower panel) immunostaining 48h-PE of EZH2DSET, EZH2 or empty vector in HH16 chick embryos. Graphics show quantification of LHX2/9+ (upper) and dorsal ISL1/2+ (lower) cells on electroporated (GFP+) versus non-electroporated side. Data show mean of n=30-35 sections (from 4-6 embryos). Error bars indicate s.d. *$p<0.05$; ***$p<0.0001$.

(B) Pax6 and Pax7 immunostaining 24h-PE of BMP7, BMP7 and EZH2DSET or BMP7 and EZH2 in HH10 chick embryos.

**Figure 4. Noggin expression is regulated by H3K27me3**

(A) Diagram summarizing experimental procedure before microarray analysis. HH10 embryos were electroporated with the empty vector or EZH2DSET (bicistronic vector containing GFP). 24h-PE (HH16-18) neural tubes were dissected out and GFP+ cells were sorted by FACS. mRNA was extracted and retro-transcribed for microarray analysis (right) or qPCR (B). List of genes upregulated in EZH2DSET and found in GO terms relating to nervous system development (right).

(B) Noggin, Hes5 and NeuroD mRNA relative levels determined by qPCR.

(C) Hes5, Noggin and NeuroD mRNA in situ hybridization in HH16-18 embryo spinal cord (upper). ChIP assays using HH16-18 chick neural tubes were performed using anti-H3K27me3 and H3K4me2 antibodies; and their levels at Hes5, Noggin and NeuroD promoters (-2000bp from TSS) were analyzed by qPCR (lower graphs). Right graph represents the H3K27me3 occupancy relative to H3K4me2 occupancy in each promoter and the mRNA expression level of each gene in WT HH16-18 spinal cord. Relative occupancy was determined calculating the percentage of each histone mark related to

the number resulting from the addition of both histone mark levels (% input). (D) Diagram summarizing the experimental procedure to obtain cells for ChIP (upper). HH10 chick neural tubes were electroporated with the empty vector or EZH2DSET. 24h-PE (HH16-18) neural tubes were dissected out and GFP+ electroporated cells were sorted by FACS for ChIP assays. Lower graphs show H3K27me3 and H3K4me2 levels at Hes5, Noggin and NeuroD promoters (-2000bp from TSS) analyzed by qPCR. Right graph represents the H3K27me3 occupancy relative to H3K4me2 occupancy in each promoter and the mRNA expression level of each gene in EZH2DSET electroporated spinal cord cells. Relative occupancy was estimated as in (C) but using data resulting from the difference between each histone mark level in empty vector and EZH2DSET normalized to the WT levels. (A-D) Results are mean of two independent experiments. Error bars indicate s.d.

**Figure 5. BMP pathway regulates Noggin transcription *via* H3K27 demethylation**

HH10 embryos were electroporated and neural tubes were dissected out 24h-PE (A-B).

(A) Relative Noggin mRNA levels quantified by qPCR (top panel) and ISH (bottom panel) after electroporation with BMP7, BMP4, Wnt, Shh or empty vector.

(B) ChIP assays were performed as in Fig. 4C using BMP4 electroporated neural tubes. Graphs show H3K27me3 and H3K4me2 levels at Hes5, Noggin and NeuroD promoters (-2000bp from TSS) analyzed by qPCR. Right graph represents the H3K27me3 occupancy relative to H3K4me2 occupancy in each promoter and the mRNA expression level of each gene after BMP4 electroporation. Relative occupancy was estimated as in (Fig. 4C) but using data resulting from the difference between each histone mark level in empty vector and BMP4 normalized to the WT levels. (C) HH10 embryos were electroporated and 24h-PE neural tubes were dissected out for GFP+ cell sorting.

Graphs show Noggin mRNA relative levels (left) and H3K27me3 levels at Noggin promoter (-2000bp from TSS) (middle) in empty vector and BMP4 or JMJD3DN and BMP4 electroporated neural tube cells. Right graph shows JMJD3 levels at Noggin promoter (-2000bp from TSS) in empty vector, myc-JMJD3 or myc-JMJD3 and BMP4 electroporated neural tube cells. JMJD3 levels were analyzed by qPCR of DNA purified from ChIP with anti-Myc antibody (Abcam). (A-C) Results are mean of two independent experiments. Error bars indicate s.d.

**Figure 6. BMP induces pSmad1 recruitment to Noggin promoter and the interaction of Smad1/Smad4 complexes with JMJD3**

(A) HH10 neural tubes were electroporated with empty vector or BMP4 and dissected out 24h-PE. The presence of endogenous phospho-Smad1 (pSmad1) at Noggin promoter (-1000bp from TSS) analyzed by qPCR of purified DNA from ChIP.Results are mean of two independent experiments. Error bars indicate s.d.

(B, C, D) Immunoblot of CoIP experiments. Top panel indicates the transfected plasmid combination used in each line. CoIPs were performed using the anti-Myc antibody. (B) Smad1 and JMJD3 interaction in the absence or presence of Smad4. (C) Smad4 interacts with JMJD3 in presence of Smad1. (D) Smad1/Smad4 and JMJD3 interaction in the absence or presence of BMP4. IB (immunoblot); IP (immunoprecipitation). Results are representative of two independent experiments.

**Figure 7. BMP-dependent upregulation of Noggin plays a role controlling BMP activity**

(A) Id3 mRNA levels determined by qPCR of FACS separated GFP+ cells or ISH of 24h-PE dissected out embryos electroporated at HH10 with indicated plasmids. Results are mean of two independent experiments. Error bars indicate s.d.

(B) Model for Noggin regulation by H3K27me3 in developing spinal cord (see text for details).

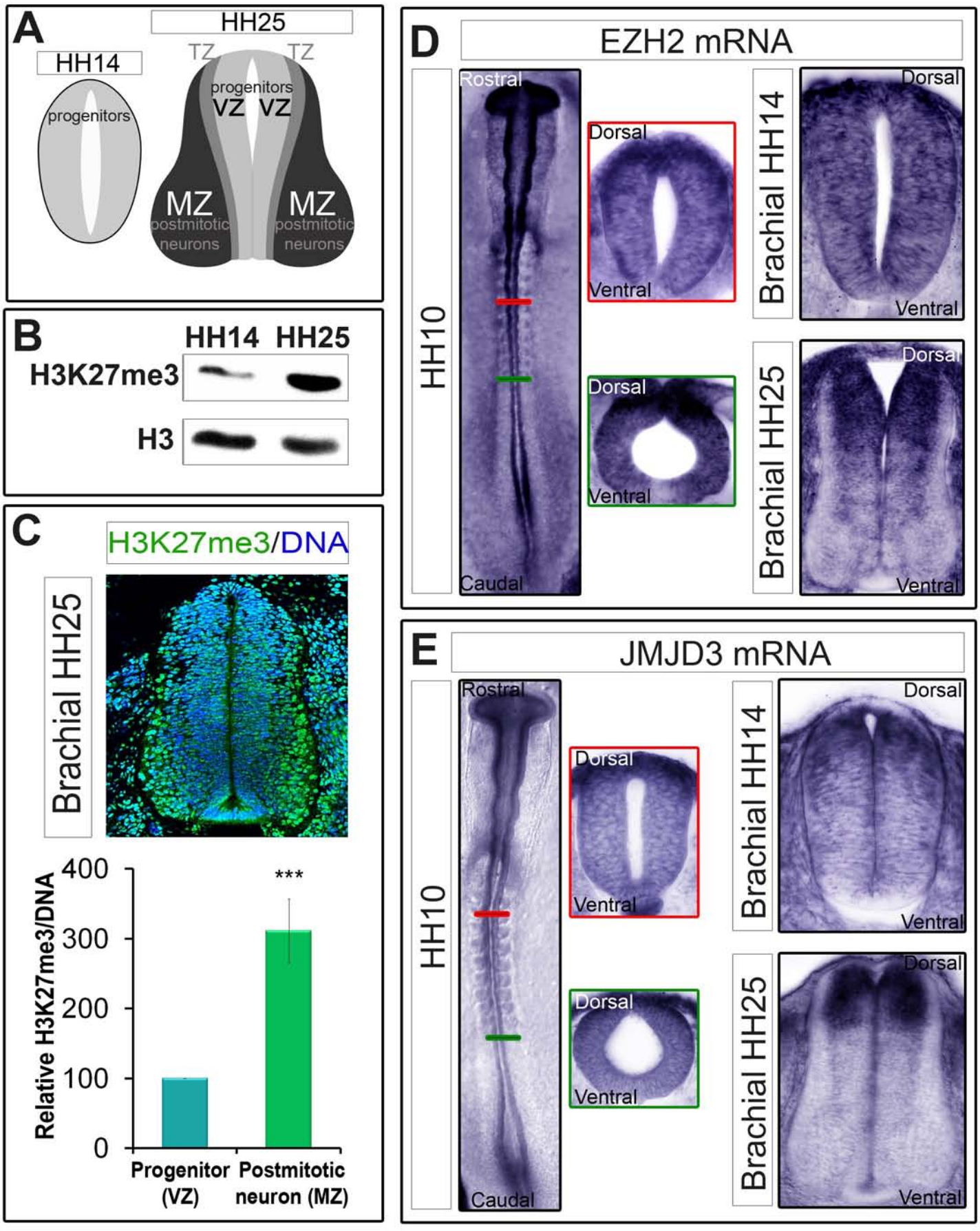
A
HH14
progenitors
HH25
TZ
TZ
progenitors
VZ VZ
MZ
postmitotic
neurons
MZ
postmitotic
neurons
B
HH14 HH25
H3K27me3
H3
C
H3K27me3/DNA
Brachial HH25
Relative H3K27me3/DNA
400
300
200
100
0
***
Progenitor (VZ)
Postmitotic neuron (MZ)
D
EZH2 mRNA
HH10
Rostral
Caudal
Dorsal
Ventral
Dorsal
Ventral
Brachial HH14
Dorsal
Ventral
Brachial HH25
Dorsal
Ventral
E
JMJD3 mRNA
HH10
Rostral
Caudal
Dorsal
Ventral
Dorsal
Ventral
Brachial HH14
Dorsal
Ventral
Brachial HH25
Dorsal
Ventral

Fig_2

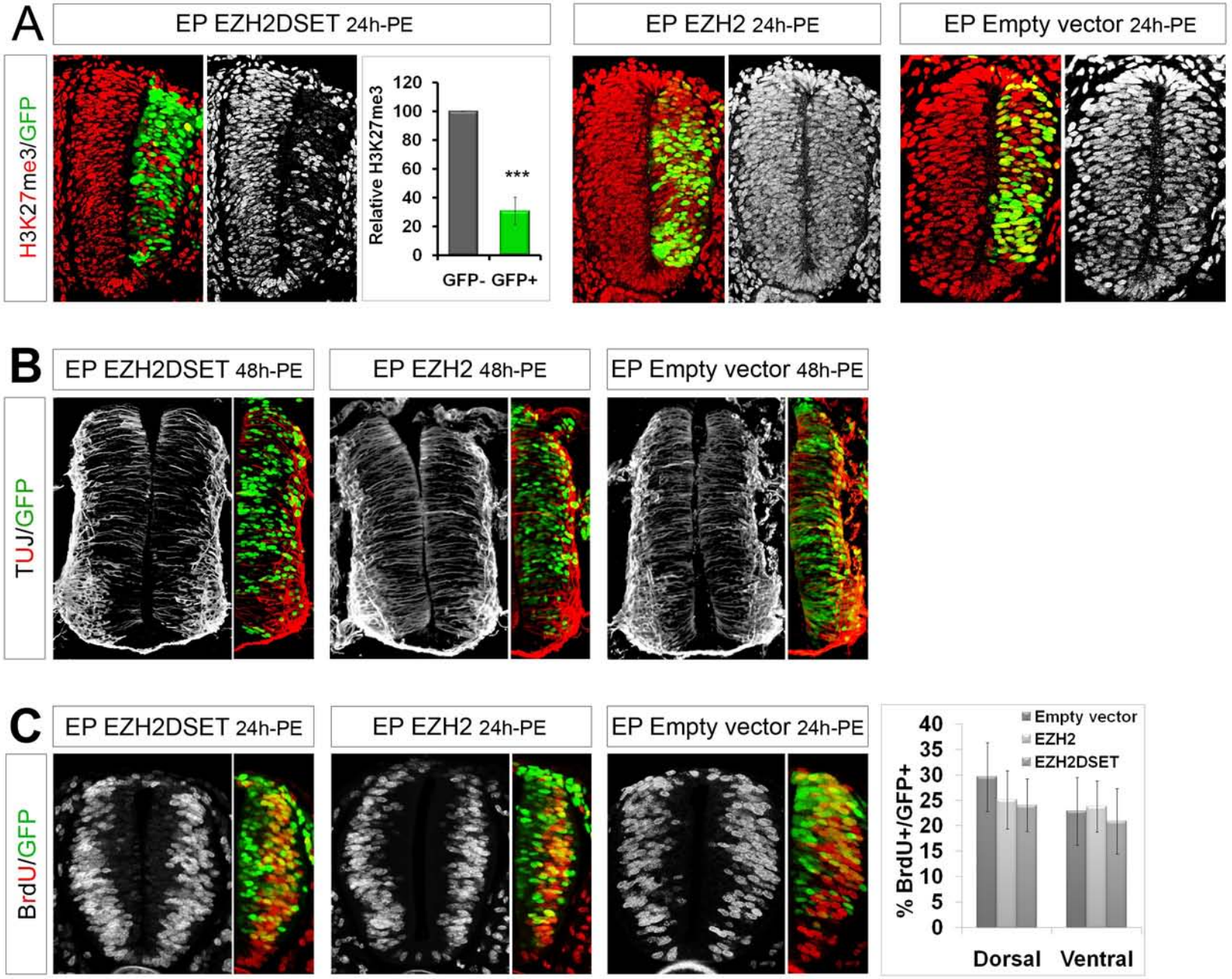
A
EP EZH2DSET 24h-PE
EP EZH2 24h-PE
EP Empty vector 24h-PE
H3K27me3/GFP
Relative H3K27me3
120
100
80
60
40
20
0
***
GFP- GFP+
B
EP EZH2DSET 48h-PE
EP EZH2 48h-PE
EP Empty vector 48h-PE
TUJ/GFP
C
EP EZH2DSET 24h-PE
EP EZH2 24h-PE
EP Empty vector 24h-PE
BrdU/GFP
% BrdU+/GFP+
40
35
30
25
20
15
10
5
0
Empty vector
EZH2
EZH2DSET
Dorsal
Ventral

Fig_3

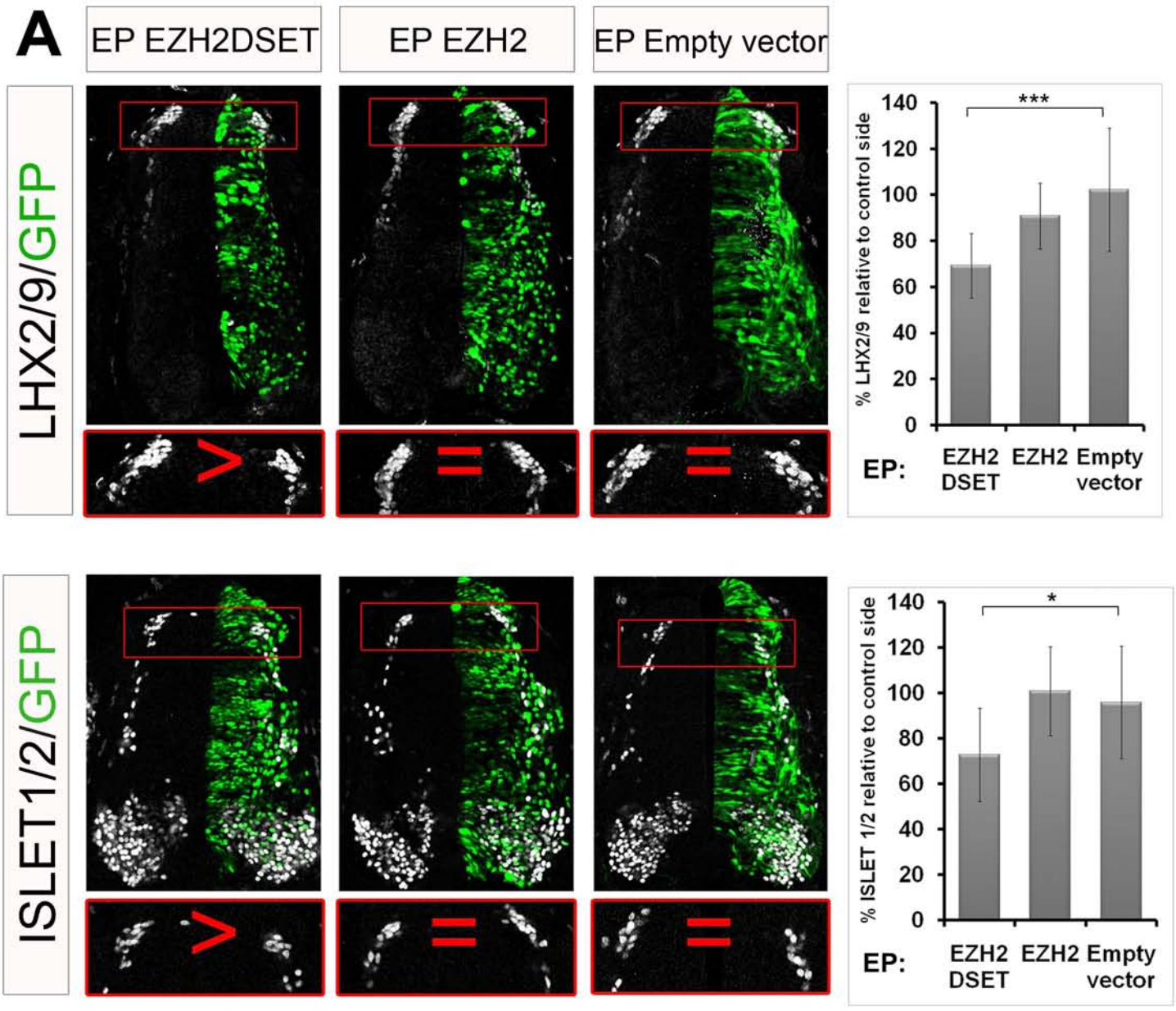
A
EP EZH2DSET
EP EZH2
EP Empty vector
LHX2/9/GFP
% LHX2/9 relative to control side
***
EP:
EZH2 DSET
EZH2
Empty vector
ISLET1/2/GFP
% ISLET 1/2 relative to control side
*
B
EP BMP7
EP EZH2DSET +BMP7
EP EZH2 +BMP7
PAX7/PAX6/GFP

Fig_4

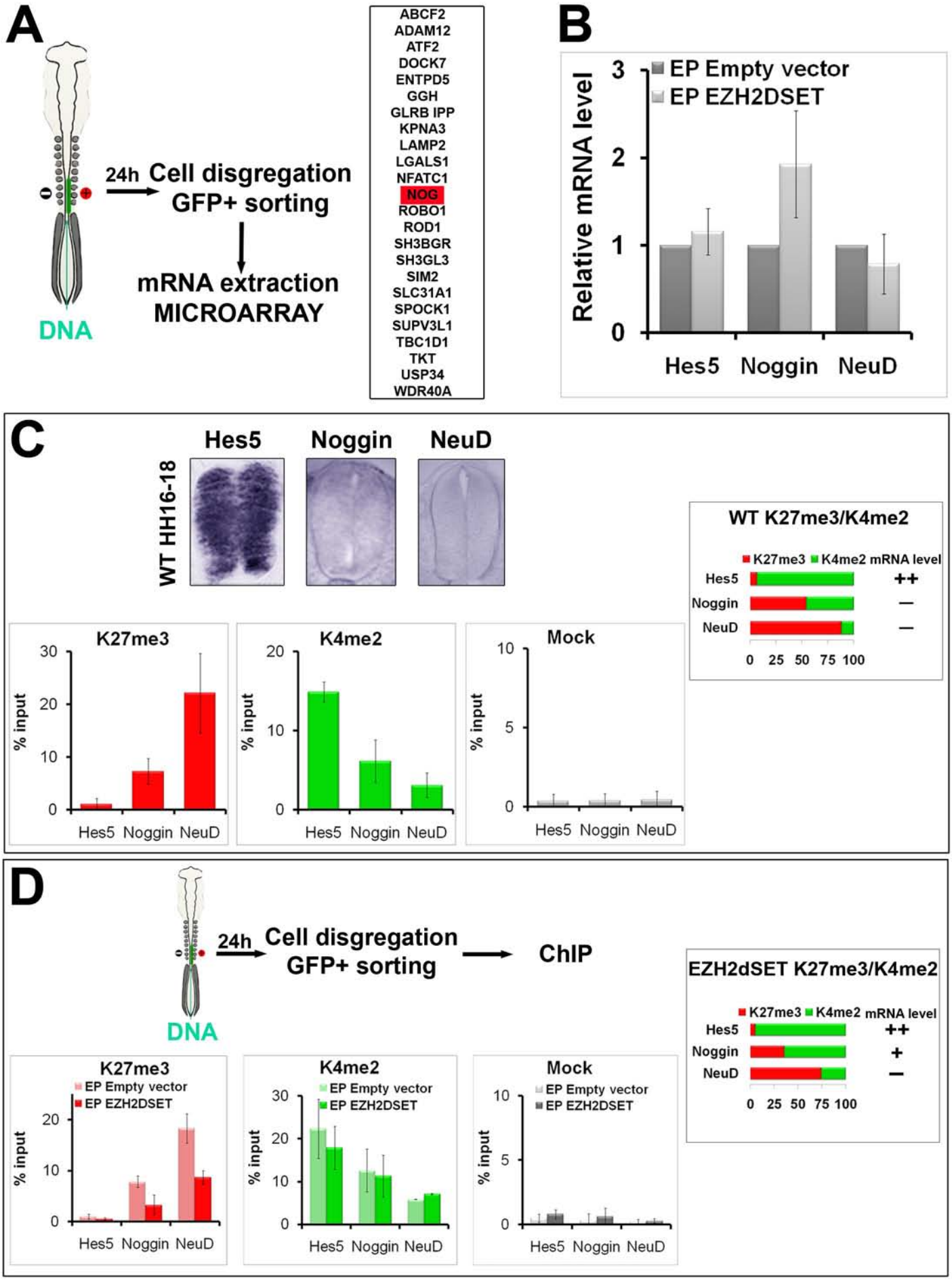
A
24h Cell disgregation
GFP+ sorting
mRNA extraction
MICROARRAY
DNA
ABCF2
ADAM12
ATF2
DOCK7
ENTPD5
GGH
GLRB IPP
KPNA3
LAMP2
LGALS1
NFATC1
NOG
ROBO1
ROD1
SH3BGR
SH3GL3
SIM2
SLC31A1
SPOCK1
SUPV3L1
TBC1D1
TKT
USP34
WDR40A
B
EP Empty vector
EP EZH2DSET
Relative mRNA level
Hes5 Noggin NeuD
C
Hes5
Noggin
NeuD
WT HH16-18
WT K27me3/K4me2
K27me3 K4me2 mRNA level
Hes5 ++
Noggin —
NeuD —
K27me3
K4me2
Mock
% input
Hes5 Noggin NeuD
D
24h Cell disgregation
GFP+ sorting
ChIP
DNA
EZH2dSET K27me3/K4me2
K27me3 K4me2 mRNA level
Hes5 ++
Noggin +
NeuD —
EP Empty vector
EP EZH2DSET

Fig_5

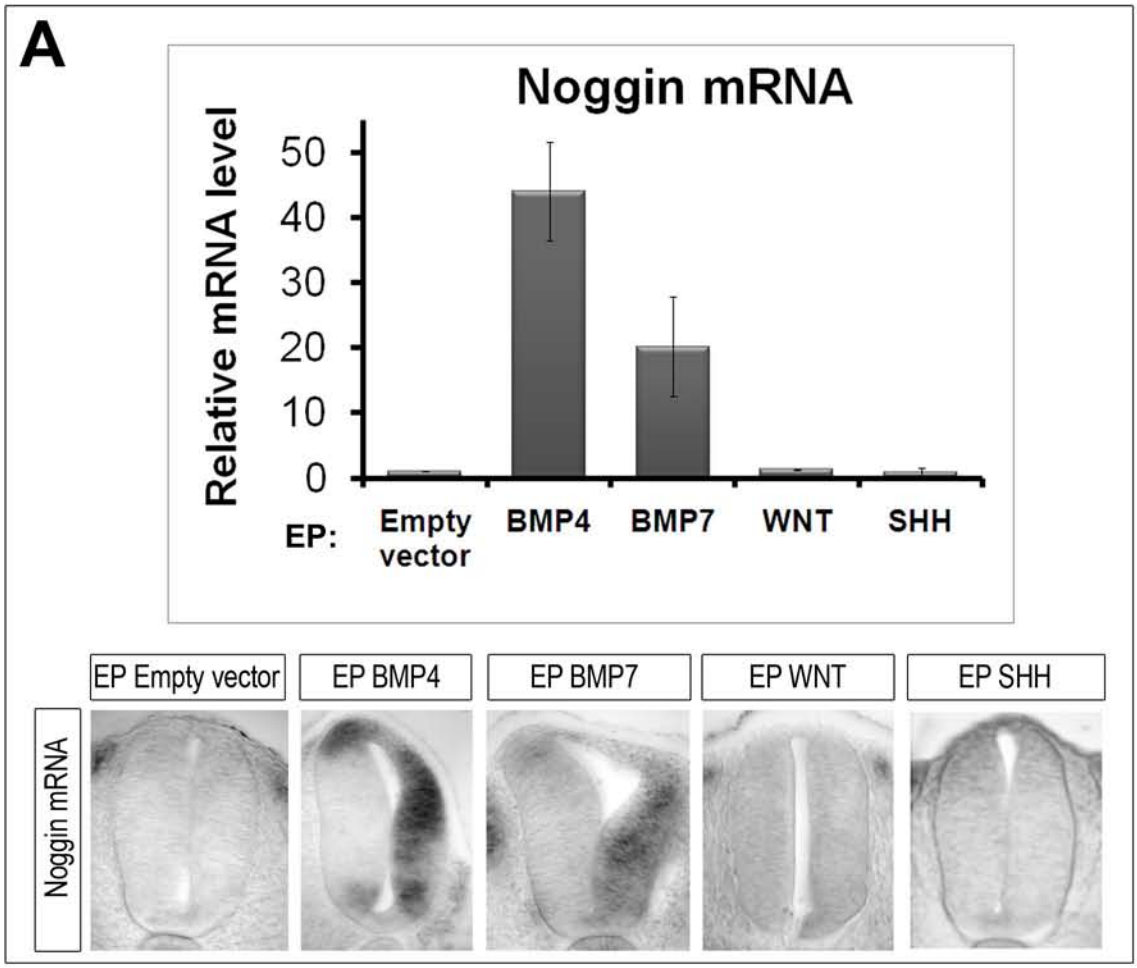
A
Noggin mRNA
Relative mRNA level
50
40
30
20
10
0
EP:
Empty vector
BMP4
BMP7
WNT
SHH
EP Empty vector
EP BMP4
EP BMP7
EP WNT
EP SHH
Noggin mRNA

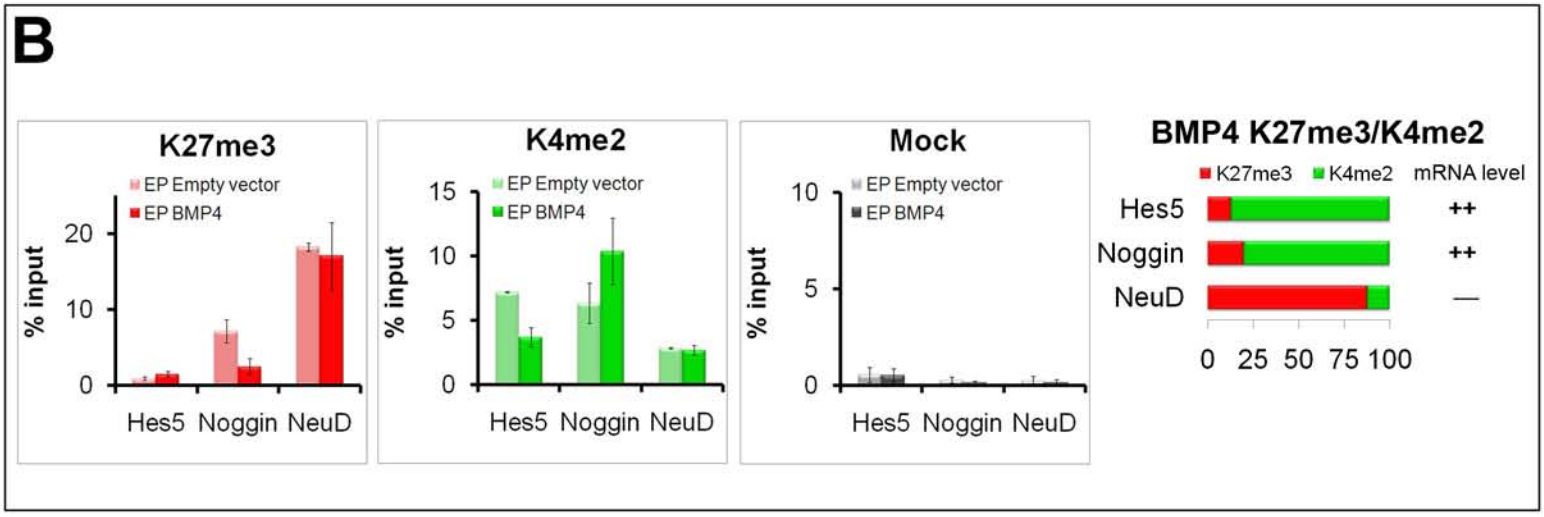
B
K27me3
EP Empty vector
EP BMP4
% input
20
10
0
Hes5 Noggin NeuD
K4me2
EP Empty vector
EP BMP4
% input
15
10
5
0
Hes5 Noggin NeuD
Mock
EP Empty vector
EP BMP4
% input
10
5
0
Hes5 Noggin NeuD
BMP4 K27me3/K4me2
K27me3
K4me2
mRNA level
Hes5
Noggin
NeuD
++
++
—
0 25 50 75 100

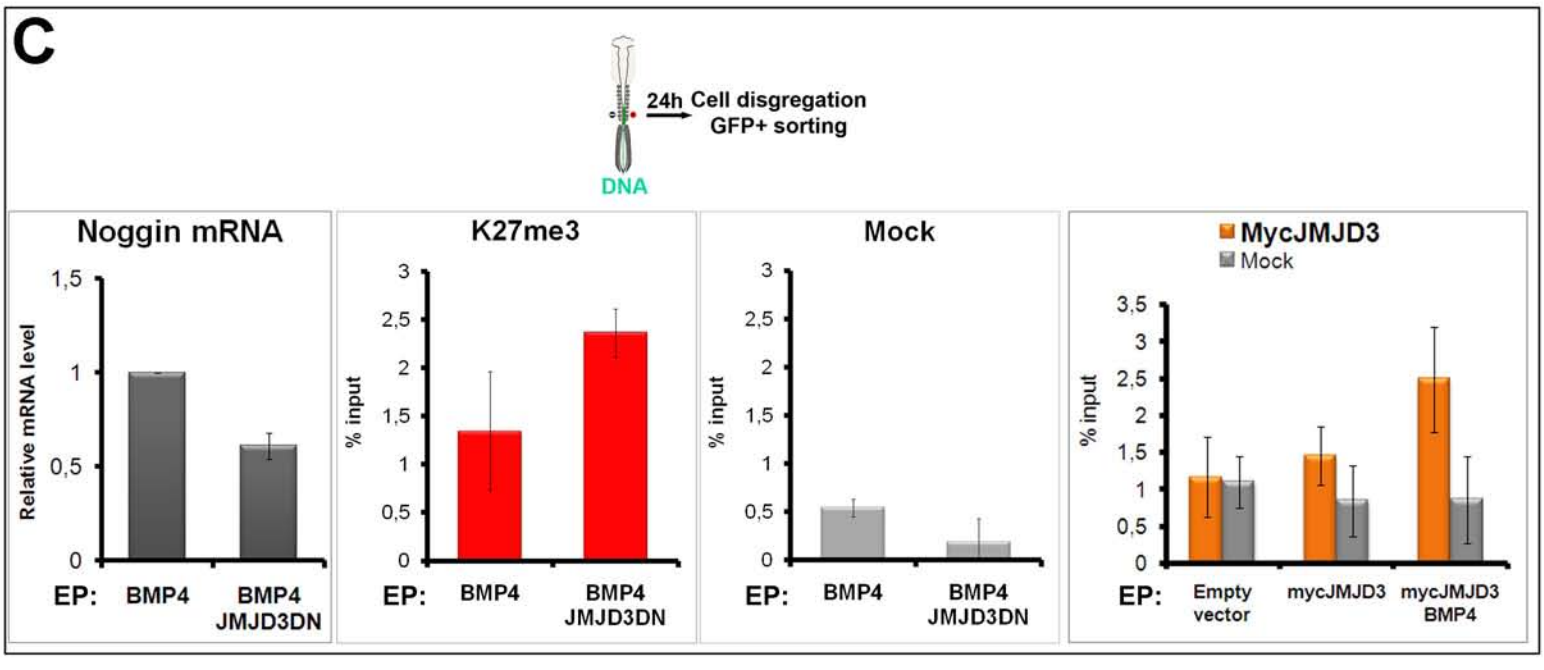
C
24h Cell disgregation
GFP+ sorting
DNA
Noggin mRNA
Relative mRNA level
1,5
1
0,5
0
EP:
BMP4
BMP4 JMJD3DN
K27me3
% input
3
2,5
2
1,5
1
0,5
0
EP:
BMP4
BMP4 JMJD3DN
Mock
% input
3
2,5
2
1,5
1
0,5
0
EP:
BMP4
BMP4 JMJD3DN
MycJMJD3
Mock
% input
3,5
3
2,5
2
1,5
1
0,5
0
EP:
Empty vector
mycJMJD3
mycJMJD3 BMP4

Fig_6

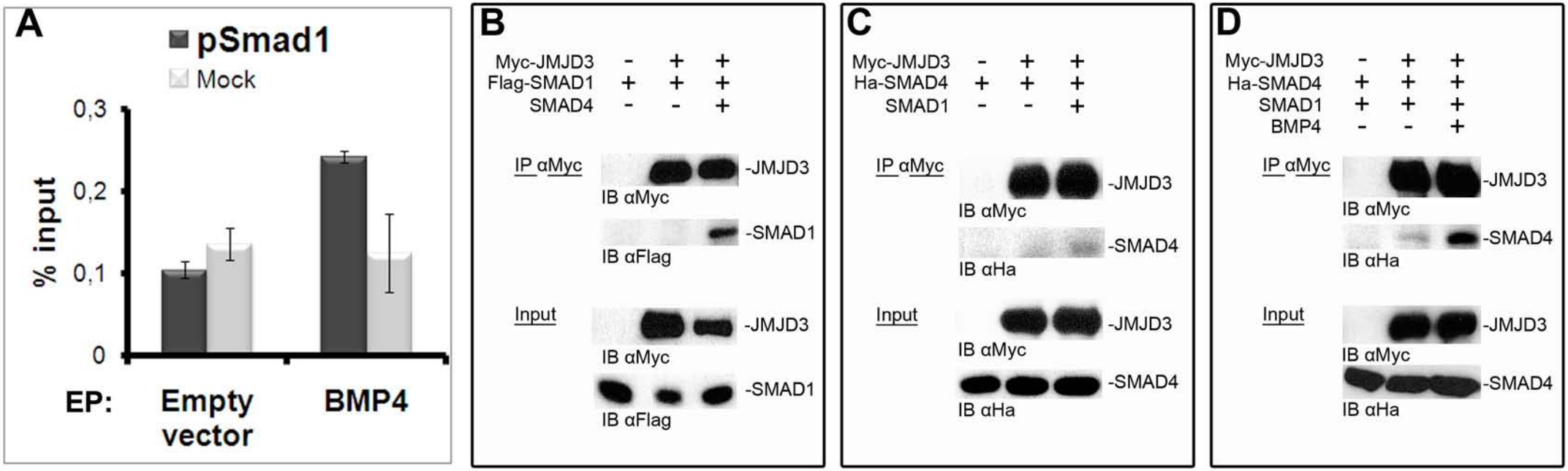
A
pSmad1
Mock
0,3
0,2
0,1
0
% input
EP:
Empty vector
BMP4
B
Myc-JMJD3 - + +
Flag-SMAD1 + + +
SMAD4 - - +
IP αMyc
-JMJD3
IB αMyc
-SMAD1
IB αFlag
Input
-JMJD3
IB αMyc
-SMAD1
IB αFlag
C
Myc-JMJD3 - + +
Ha-SMAD4 + + +
SMAD1 - - +
IP αMyc
-JMJD3
IB αMyc
-SMAD4
IB αHa
Input
-JMJD3
IB αMyc
-SMAD4
IB αHa
D
Myc-JMJD3 - + +
Ha-SMAD4 + + +
SMAD1 + + +
BMP4 - - +
IP αMyc
-JMJD3
IB αMyc
-SMAD4
IB αHa
Input
-JMJD3
IB αMyc
-SMAD4
IB αHa

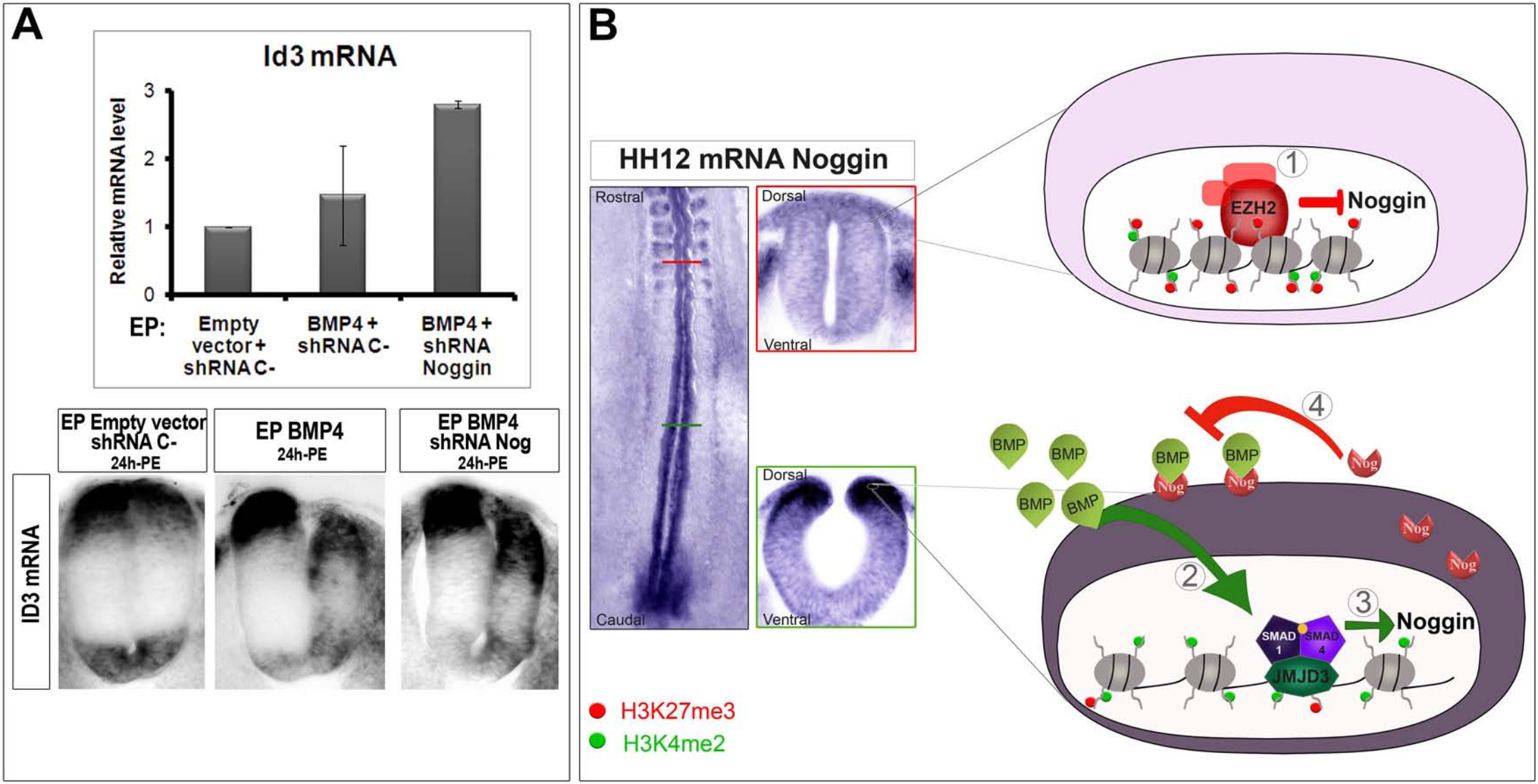
A
Id3 mRNA
Relative mRNA level
3
2
1
0
EP:
Empty vector + shRNA C-
BMP4 + shRNA C-
BMP4 + shRNA Noggin
EP Empty vector shRNA C- 24h-PE
EP BMP4 24h-PE
EP BMP4 shRNA Nog 24h-PE
ID3 mRNA
B
HH12 mRNA Noggin
Rostral
Caudal
Dorsal
Ventral
Dorsal
Ventral
H3K27me3
H3K4me2
1
EZH2
Noggin
4
BMP
Nog
2
3
SMAD 1
SMAD 4
JMJD3
Noggin